Permanent Magnet Synchronous Generator-Based Standalone Wind Energy Supply System

C. N. Bhende, S. Mishra, *Senior Member, IEEE*, and Siva Ganesh Malla

Abstract—In this paper, a novel algorithm, based on dc link voltage, is proposed for effective energy management of a standalone permanent magnet synchronous generator (PMSG)-based variable speed wind energy conversion system consisting of battery, fuel cell, and dump load (i.e., electrolyzer). Moreover, by maintaining the dc link voltage at its reference value, the output ac voltage of the inverter can be kept constant irrespective of variations in the wind speed and load. An effective control technique for the inverter, based on the pulsewidth modulation (PWM) scheme, has been developed to make the line voltages at the point of common coupling (PCC) balanced when the load is unbalanced. Similarly, a proper control of battery current through dc–dc converter has been carried out to reduce the electrical torque pulsation of the PMSG under an unbalanced load scenario. Based on extensive simulation results using MATLAB/SIMULINK, it has been established that the performance of the controllers both in transient as well as in steady state is quite satisfactory and it can also maintain maximum power point tracking.

Index Terms—DC-side active filter, permanent magnet synchronous generator (PMSG), unbalanced load compensation, variable speed wind turbine, voltage control.

I. INTRODUCTION

IN wind energy application, variable speed wind turbines are popular mainly because of their capability to capture more power from the wind using the maximum power point tracking (MPPT) algorithm and improved efficiency [1]. Presently, doubly feed induction generators (DFIGs) are widely used as the generator in a variable speed wind turbine system. In case of DFIG, there is a requirement of the gearbox to match the turbine and rotor speed. The gearbox many times suffers from faults and requires regular maintenance [2], making the system unreliable. The reliability of the variable speed wind turbine can be improved significantly using a direct drive-based permanent magnet synchronous generator (PMSG). PMSG has received much attention in wind energy applications because of its self-excitation capability, leading to a high power factor and high efficiency operation [3].

In many countries, there are remote communities where connection with the power grid is too expensive or impractical and diesel generators are often the source of electricity. Under such circumstances, a locally placed small-scale standalone
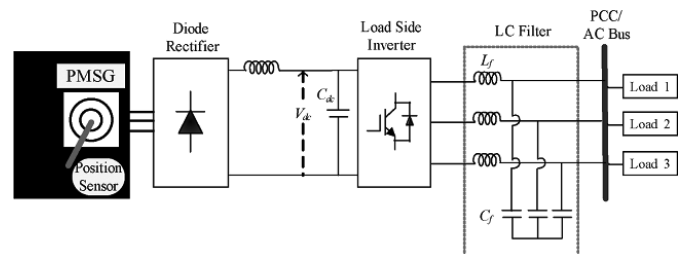
Fig. 1. Standalone wind energy system.

distributed generation system can supply power to the customers. Autonomous wind power systems are among the most interesting and environment friendly technological solutions for the electrification of remote consumers.

The control of an inverter to present the customers with a balanced supply voltage is the main challenge in a standalone system. Moreover, voltage variations, flickers, harmonic generation, and load unbalance are the major power quality (PQ) problems that occur in the wind energy conversion system (WECS). The voltage variations are mainly due to the change in load. Flicker or voltage fluctuations are primarily caused by variations in the power from WECS which comes into existence, owing to the fluctuations in the wind speed. Unwanted harmonics are generated due to the power electronics interface (rectifier, inverter and dc–dc converter) between the wind generator and the load. Those power quality problems may not be tolerated by the customers and hence require mitigation techniques.

The schematic of the standalone system using PMSG-based wind turbine is shown in Fig. 1. Such a standalone wind energy system using PMSG is already being developed in [4]–[6]. In [4], the authors have not discussed the use of an energy storage device which is required to meet the power demand in the condition of low wind speed. Similarly, in [5] and [6], the authors are silent about the effect of unbalanced load which is a common phenomenon in the distribution network. Due to unbalanced load, the voltages at point of common coupling (PCC) become unbalanced. Moreover, unbalanced load will create pulsation in the generator torque which will reduce the life of the turbine shaft.

In this paper, using battery and fuel cell along with aqua electrolyzer as the storage devices, a small-scale standalone power supply system based on wind energy is considered. Our objectives are:

a) To achieve effective control coordination among the wind generator, battery, fuel cell, and aqua electrolyzer to maintain the dc-link voltage constant.
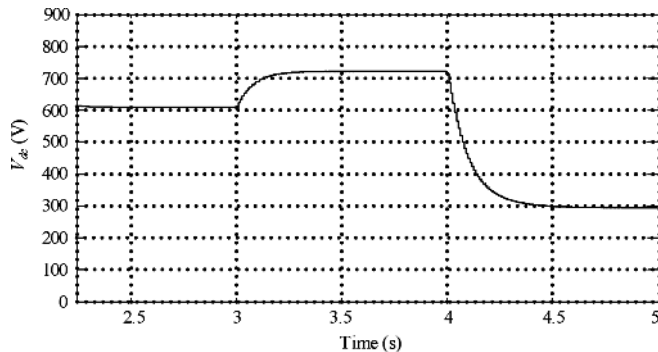
Fig. 2.   DC link voltage without battery.

b) To maintain constant and balanced voltages at the ac bus (or load bus) as three phase dynamic loads need a balanced three-phase supply for their proper operation.

c) To reduce the effect of unbalanced load current on the torque pulsation of PMSG.

II. CONTROL OF PROPOSED WIND ENERGY SYSTEM IN STANDALONE MODE

In standalone mode, the output ac voltage is controlled in terms of amplitude and frequency. Power from the PMSG-based wind turbine is fed to ac–dc–ac converters to maintain the output ac voltage at specified amplitude and frequency. The variations in the wind speed as well as in the load affect the dc link voltage (V_{dc}) between rectifier and inverter. This is illustrated in Fig. 2 which is a plot of V_{dc} in response to the change in wind speed and load without connecting battery. In Fig. 2, at $t = 3$ s, V_{dc} increases due to the reduction in load from 5 to 2.5 kW by keeping wind speed constant at 12 m/s. Similarly, the effect of decrease in wind speed from 12 to 7 m/s on V_{dc} can be observed at $t = 4$ s. Hence, it is concluded that the dc link voltage (V_{dc}) is directly affected because of any kind of variation in wind speed as well as load. Therefore, if V_{dc} is maintained constant at its reference value and keeping the modulation index of load side inverter at 1, the amplitude of output ac voltage can be controlled and maintained at the rated voltage. This is explained below:

The relation between dc voltage and output ac voltage of three-phase pulsewidth modulation (PWM) inverter is given by [7]

$$V_{LL_1} = \frac{\sqrt{3}}{2\sqrt{2}} k\, V_{dc} \tag{1}$$

where

V_{LL_1} = Fundamental phase-phase root-mean-square (rms) voltage on the ac side;
k = Modulation index of the PWM inverter;
V_{dc} = the dc link voltage.

From (1), it is seen that the ac voltage can be maintained at rated value by maintaining V_{dc} at its reference value and with $k = 1$. As far as frequency of output ac voltage is concerned, it can be maintained at a specified value by choosing the frequency of sinusoidal reference signal while generating the PWM pulses.

III. CONTROL OF DC LINK VOLTAGE

The proposed standalone PMSG-based wind turbine power system is shown in Fig. 3. Neutral wire is provided between the capacitors connected before the inverter, as shown in Fig. 3. By providing the neutral system, we can feed to both single-phase as well as three-phase loads. The battery is connected to the dc link through a dc–dc bidirectional buck-boost converter. Using a bidirectional buck-boost converter, the battery voltage can be kept lower as compared to reference dc link voltage (V_{dc}^*) and hence fewer batteries need to be connected in series. In the proposed system, battery voltage is kept at about 300 V while $V_{dc}^* = 640$ V. In this paper, the rating of the battery bank, considering 60% depth of discharge (DOD) [8], is decided based on the assumption that even when the wind power is zero and fuel cell is under maintenance, it should cater to the energy requirement of a 6-kW load for approximately an hour. The detail about the calculation of the battery rating is discussed in Appendix I.

The schematic of the dc–dc converter controller used to regulate the charging/discharging current of the battery to maintain the dc bus voltage constant is depicted in Fig. 4. Treating the controller output as the reference current for the battery, a hysteresis band approach is adapted to switch either Q_1 or Q_2 of the dc–dc converter (Fig. 3). In addition, the control signal is constrained within a limit so that the actual charging/discharging current will be as per the specification of the battery; as a result the longevity of the battery will be enhanced.

A proper real power management scheme needs to be formulated to maintain the dc bus voltage constant to keep modulation index within a reasonably practical limit, when the ac output voltage (PCC voltage) of the inverter needs to be maintained constant. In our system (Fig. 3), apart from wind there are three other devices, namely battery, fuel cell, and dump load (i.e., electrolyzer). Out of the three equipments, the battery can act either as a source or as a sink. As a result it should discharge (charge) within specified limits when there is deficit (surplus) of wind energy due to low (high) wind speed. The fuel cell can only act as a source when sufficient hydrogen is available to us. Similarly, an aqua electrolyzer can only act as a sink for the system. In this work, it is assumed that, due to high wind speed, the excess energy produced is first pushed into the battery until it reaches its upper limit of charge carrying capacity and then the excess power is fed to the electrolyzer and is regulated via the chopper control (switch S_d in Fig. 3). The decision about switching on the control action is carried out by comparing the upper limit of the state of charge (SOC) of the battery and the present status of SOC. When the SOC becomes higher than its limit, the controller will increase the duty cycle as a function of over voltage in the dc bus voltage. The schematic of the control scheme is depicted in Fig. 5.

In case of a long-term no-wind or low-wind condition, the battery alone may not cater to the load demand. Hence, the fuel cell is integrated with WECS. The fuel cell can meet the load demand in steady state; however, due to its slow dynamics it cannot feed the power instantaneously and hence is unable to stabilize the dc link voltage during transients. Therefore, proper coordination and control is required between the battery and fuel cell. Fig. 6 shows the fuel cell controller through which the
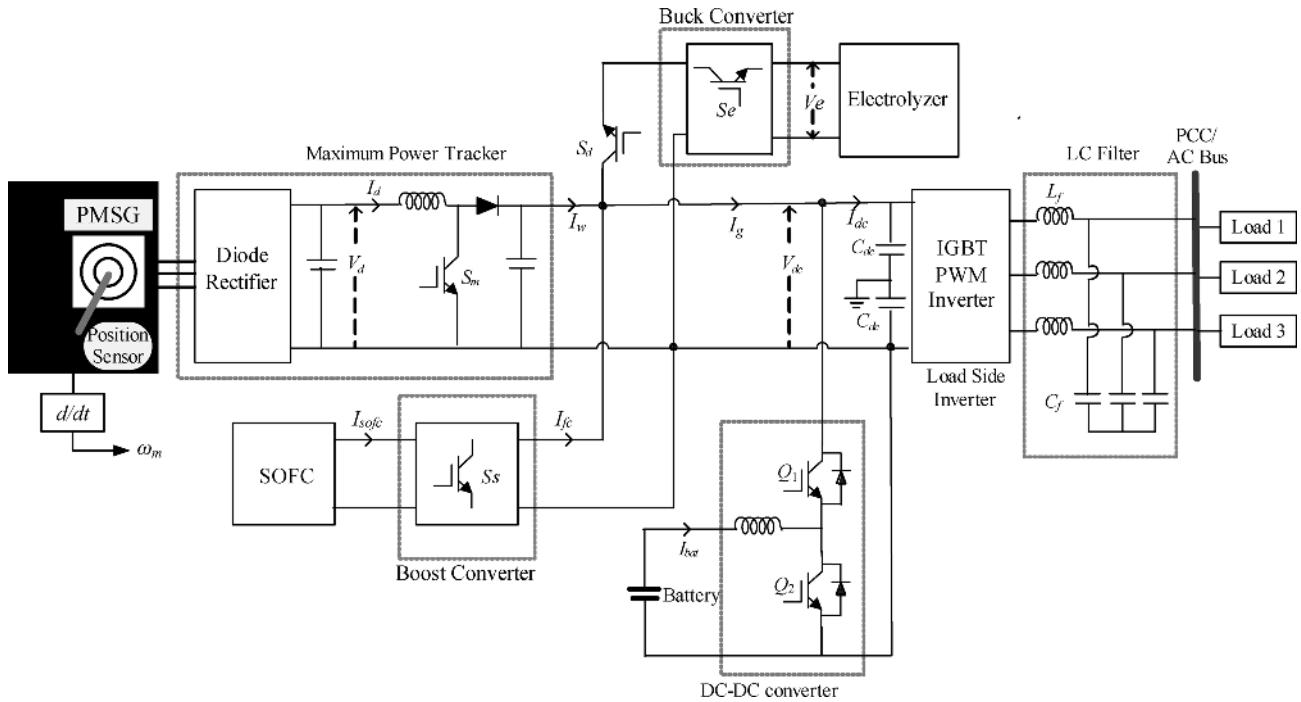
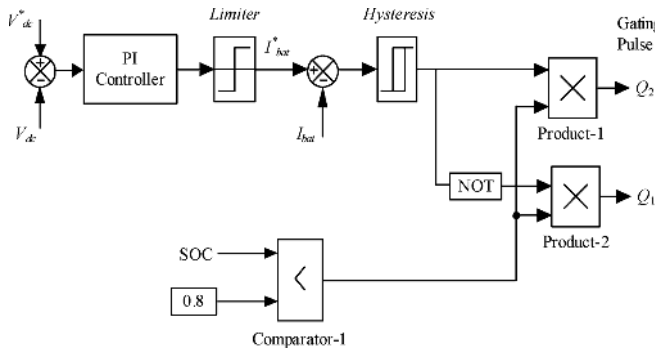Fig. 3. PMSG-based standalone wind turbine with energy storage and dump load.

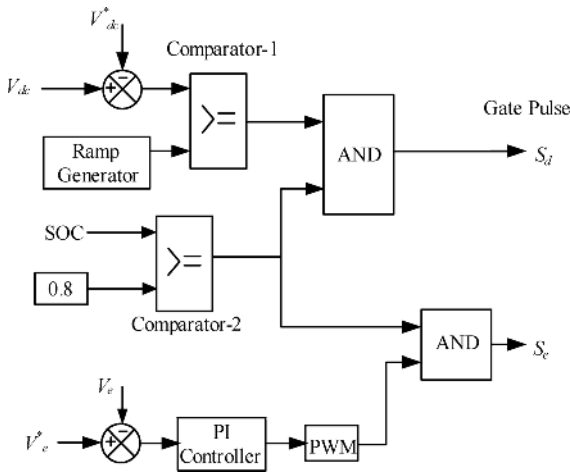

Fig. 4. DC–DC converter controller.

Fig. 6. Boost converter controller associated with fuel cell.

Fig. 5. Dump load controller.

boost converter switch S_s is controlled. Controllers associated with the battery and fuel cell are developed in such a fashion
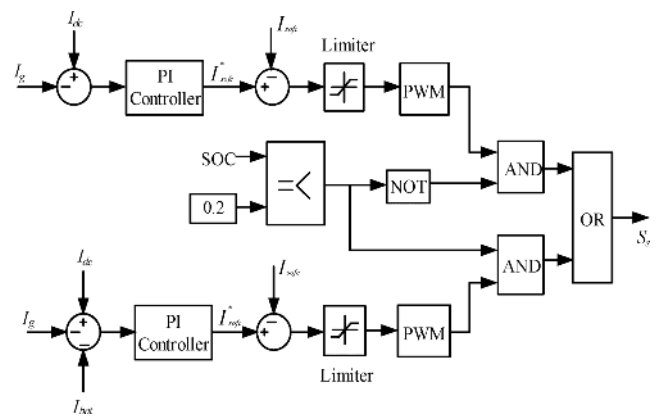
that when there is a sudden load change, the battery provides the power instantaneously and as fuel cell power goes on increasing, battery power should go on decreasing. In order to make the proper coordination between battery and fuel cell, boost converter controller (Fig. 6) associated with fuel cell is developed based on I_g and I_d (shown in Fig. 3) and assuming battery current is ideally zero. Moreover, when SOC of the battery is below 0.2, the fuel cell should give power to the battery. This facility is also provided in the fuel cell controller, as shown in Fig. 6.

A flowchart of the above discussed energy management system is depicted in Fig. 7, where the upper and lower limit for the SOC of the battery is kept at 0.2 and 0.8, respectively [8].

The control strategy based on switched mode rectifier [5], [6], [9], [10] is adapted for extracting the maximum power from wind flow when a PMSG is incorporated as the generator. The detailed theory and algorithm for maximum power extraction using measurement of turbine speed (ω_t) is explained in [5]
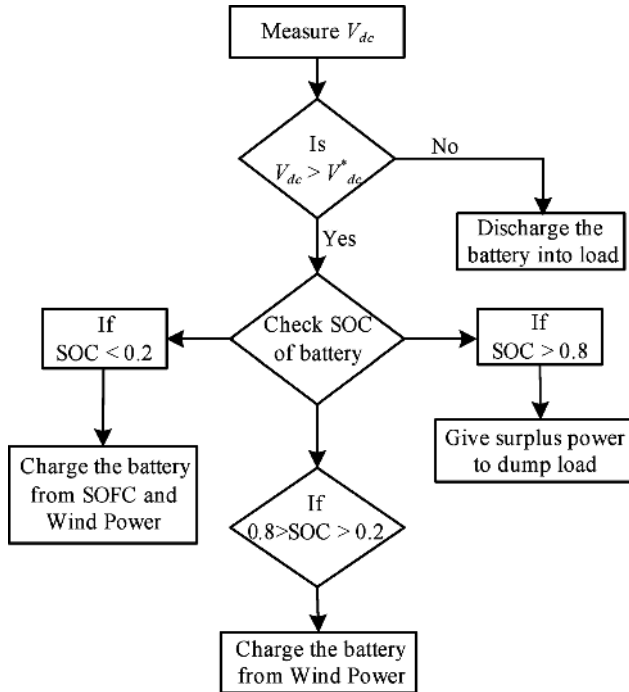
Fig. 7. Energy management algorithm.

Fig. 8. DC–DC converter controller for unbalanced load.

and [6] and hence it is not mentioned here. The load side PWM-based inverter will generate unwanted high frequency harmonics (based on the switching frequency) in the output ac voltage, which is ultimately supplied to the customer, creating a power quality problem. In this case, the switching frequency (f_s) of the PWM inverter is considered as 3 kHz. PWM switching at 3 kHz produces high-frequency harmonics that can be eliminated using simple passive LC filter. The design of the LC filter [11] is given in Appendix II and the values so obtained are

$$L_f = 4.6 \text{ mH} \quad \text{and} \quad C_f = 9 \, \mu\text{F}.$$

IV. UNBALANCED LOAD CURRENT COMPENSATION

In distribution systems, as the loads are mostly single phase in nature, the current in different phases will not be the same in magnitude and the phase difference between them may not be 120°. The detrimental effects of this unbalanced current on the generating system are
1) electrical torque pulsation;
2) unbalanced voltages at PCC.
The effect and control of the above-mentioned two quantities are discussed below.

A. Effect on the Generator Torque and Its Compensation

It has already been established in the literature [12] that when an inverter supplies unbalanced load current, the time variation of the dc link current (I_d) and dc link voltage (V_{dc}) can be expressed as a dc component superimposed with a second-harmonic component. Due to the second-harmonic component
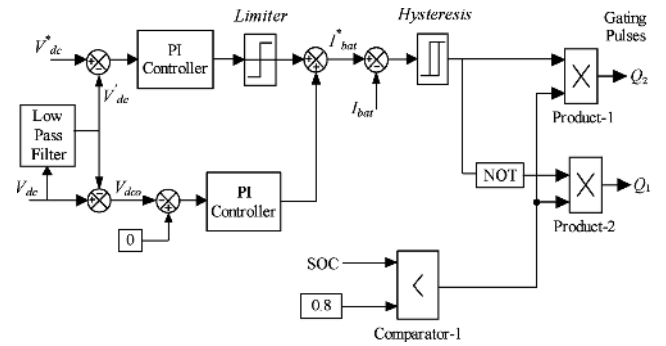
present in the dc current, the electrical torque of the generator will oscillate and the life of the turbine shaft will reduce. In this paper, a dc-side active filter is developed to reduce the oscillations in the electrical torque of the generator. The dc-side active filter [13] is implemented through a dc–dc converter connected between the dc bus and the battery.

The dc link voltage is filtered by a low-pass filter to obtain the dc component (V'_{dc}) and subtracting V'_{dc} from V_{dc} the oscillating component (V_{dco}) is estimated. Now the responsibility of the control scheme is to produce a reference current which needs to be followed by the battery current. Since the function of the battery current is both to maintain the dc bus voltage and to reduce the second-harmonic component, two control loops using PI controllers are formulated. First, a PI controller considering $(V^*_{dc} - V'_{dc})$ as error produces a reference current to maintain the dc bus voltage, whereas and the second one uses $(0 - V_{dco})$ as its error. The reference for the second one is taken as "0" as the controller should make the oscillating component in the dc voltage to "0." The outputs of both the PI controllers are added to generate the final reference battery current (I^*_{bat}). The reference battery current so obtained is then compared with the actual battery current (I_{bat}) and the error is processed through a hysteresis band which in turn gives control signals (gating pulses) to the IGBT devices $(Q_1$ and $Q_2)$ of the dc–dc converter. Therefore, the dc–dc converter control discussed in Section III is modified based on the above discussion to take care of the unbalance load and is presented in Fig. 8.

B. Effect on Voltage at PCC and Its Compensation

Due to unbalanced load being connected to the inverter, the current in each phase will not be equal, leading to unequal voltage drop across LC filters used in each phase. This unbalanced voltage drop will cause the line voltages at PCC to become unbalanced and the voltage unbalance factor (i.e., ratio of negative sequence to positive sequence of fundamental component) may not be within permissible limit (i.e., below 1%). Hence, it is necessary to compensate the voltage unbalance at PCC. To achieve this goal the error between the rms (or peak) value of the phase voltages at PCC and the reference phase voltage is given to a PI controller. The output of the PI controller is multiplied with a unit sine wave generator to get the reference phase voltages $(v_{a\_ref}, v_{b\_ref}, v_{c\_ref})$. Using v_{a_ref}, v_{b_ref} and v_{c_ref}, PWM pulses are generated to switch
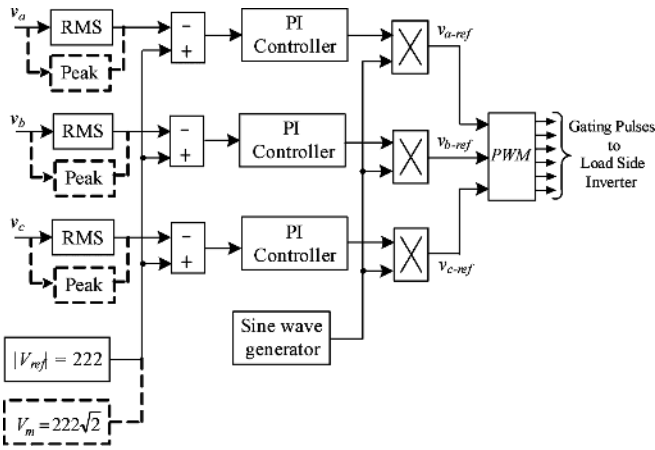
Fig. 9. PWM inverter controller for unbalanced load compensation.
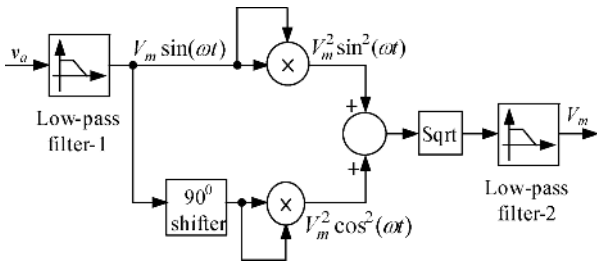

Fig. 10. Peak detection method.

ON/OFF the load side inverter. The schematic of the control scheme used for unbalanced voltage compensation is shown in Fig. 9.

Through the controller shown in Fig. 9, our aim is to get different modulation indexes for three phases so as to balance out the unbalanced PCC voltages. The controller requires the information about the actual voltage. The actual voltage can be detected by different algorithms. The detection time of both the peak detection method and $dq0$ transformation-based approach is faster than the rms measurement approach [14]. The peak detection method suggested in [14] and [15] is sensitive to small frequency variations as well as harmonics. Hence, when the peak detection method is employed to calculate v_{a_ref}, v_{b_ref} and v_{c_ref}, two low-pass filters, low-pass filter-1 (LPF-1) and low-pass filter-2 (LPF-2), are required (Fig. 10). Since voltages are measured after the inverter, they contain harmonics and hence the cutoff frequency of LPF-1 is chosen as 300 Hz [14]. In addition, as the peak detected signal still contains oscillations as depicted in Fig. 11, another low-pass filter LPF-2 is used at its output. It can be seen from Fig. 11 that when the cutoff frequency of LPF-2 is 300 Hz (same as that of LPF-1), the oscillations are more as compared to a cutoff frequency of 50 Hz. Hence, in order to capture the actual peak voltages a low-pass filter of 50 Hz need to be connected at the output of the peak detector. To evaluate the fastness of the peak detection method (along with those filters as presented in Fig. 10) and the rms-based approach, both of them are subjected to a pure sinusoidal voltage whose magnitude is reduced by 50% at $t = 1$ s, as shown in Fig. 12(a). Fig. 12(b) shows the time required for the detection by peak method along with filters (LPF-1 and LFP-2) and the rms-based method. From Fig. 12(b), it is seen that the
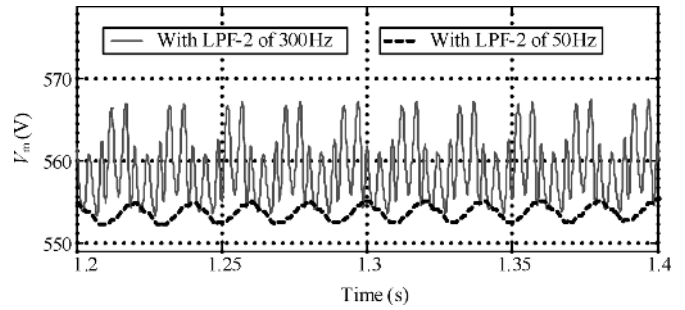

Fig. 11. Peak detected voltage after the filters.
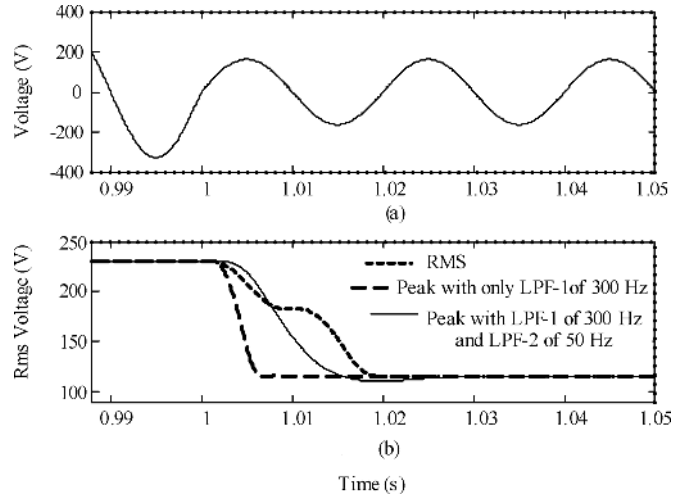

Fig. 12. (a) Measured voltage; (b) comparison of peak method along with filters and rms measurement.
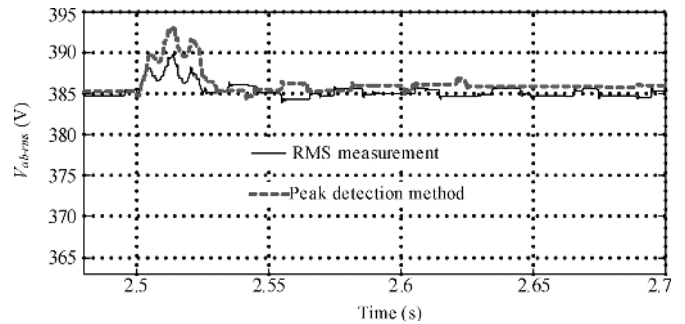

Fig. 13. Comparison of rms and peak detection method under balanced load condition.

transient time of the rms-based method is almost equal to the peak method along with LPF-1 and LFP-2.

The parameters of the PI controllers used in both approaches are tuned by the integral time square error (ITSE) method [16] for a change in load in the balanced condition. From Fig. 13, it is seen that both the controllers are showing almost the same transient response. However, when those tuned controllers are tested for unbalanced load, the response of the peak method is more sluggish as compared to the rms method which is inferred from Fig. 14.

In [17]–[19], the authors proposed integration of $dq0$ transformation and symmetrical component analysis to deal with unbalanced voltages. In this approach, sequence decomposition is carried out to get dc values after abc/dq transformation for the unbalanced voltages (Fig. 15). In the proposed system, the sensed voltages are not pure sinusoidal because they are
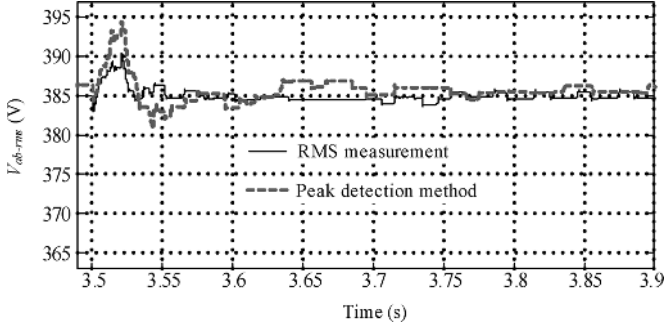
Fig. 14. Comparison of rms and peak detection method under unbalanced load condition.
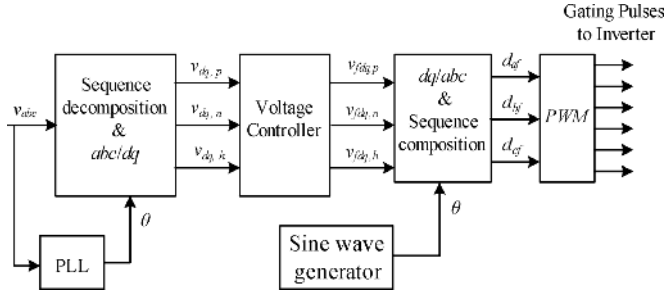

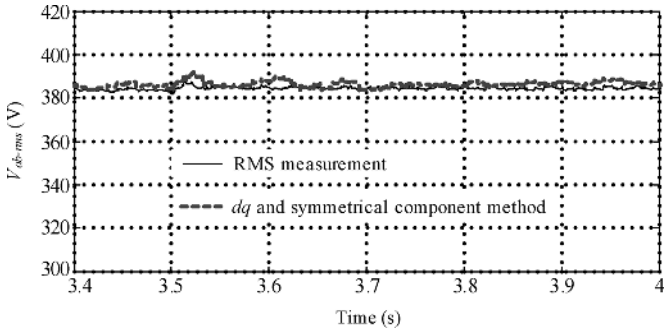Fig. 15. *dq* method integrated with symmetrical component analysis.

Fig. 16. Comparison of rms and *dq*-based symmetrical component analysis method under unbalanced load condition.

measured after the inverter and hence a low-pass filter is connected after *abc/dq* transformation. The response of the rms method and *dq* integrated with symmetrical component analysis is plotted in Fig. 16. From Fig. 16, it is seen that when unbalanced load is applied at $t = 3.5$ s, the response of line voltages is more or less the same for the two methods. The *dq* method considered is computationally intensive as there is a need to extract the symmetrical components involving complex domain calculations from the original waveforms. This may lead to a time-consuming approach when implemented in real time. Hence, in this paper, the rms-based approach is adapted to calculate the reference line voltages.

V. MODELING OF WIND TURBINE, BATTERY, FUEL CELL, AND AQUA ELECTROLYZER

A. Wind Turbine and Drive Train

In this paper, the WECS is represented with the two-mass drive train model. The differential equations governing its

mechanical dynamics are presented as follows [20]:

$$2H_t \frac{d\omega_t}{dt} = T_m - T_{sh} \tag{2}$$

$$\frac{1}{\omega_{elb}} \frac{d\theta_{tw}}{dt} = \omega_t - \omega_r \tag{3}$$

$$2H_g \frac{d\omega_r}{dt} = T_{sh} - T_g \tag{4}$$

where H_t is the inertia constant of the turbine, H_g is the inertia constant of the PMSG, θ_{tw} is the shaft twist angle, ω_t is the angular speed of the wind turbine in p.u., ω_r is the rotor speed of the PMSG in p.u., ω_{elb} is the electrical base speed, and the shaft torque T_{sh} is

$$T_{sh} = K_{sh}\theta_{tw} + D_t \frac{d\theta_{tw}}{dt} \tag{5}$$

where K_{sh} is the shaft stiffness and D_t is the damping coefficient.

B. Modeling of Battery

In this paper, a generic battery model presented in [21] is implemented. The model uses only the battery SOC as a state variable in order to avoid the algebraic loop problem and can accurately represent four types of battery chemistries including lead acid battery.

The modeling is attempted using a simple controlled voltage source with a constant resistance as shown in Fig. 17, where the controlled voltage source is described through (6)

$$E = E_0 - K \frac{Q}{Q - \int i\, dt} + A \exp\left(-B \int i\, dt\right) \tag{6}$$

$$V_{batt} = E - RI_{batt} \tag{7}$$

where

E_0	= no-load battery voltage (V);
K	= polarization voltage (V);
Q	= battery capacity (Ah);
$\int idt$	= charge drawn/supplied by the battery (Ah);
A	= exponential zone amplitude (V);
B	= exponential zone time constant inverse (Ah) $^{-1}$;
V_{bat}	= battery voltage (V);
R_{batt}	= internal resistant (Ω);
I_{batt}	= battery current (A).

C. Solid Oxide Fuel Cell (SOFC)

The SOFC model is developed in [22] and [23], and based on Nernst's equation and Ohm's law, the fuel cell stack output voltage (V) is represented (Fig. 18). For MATLAB simulation, representation of stack output voltage (V) is then connected to the controlled voltage source as shown in Fig. 18. The SOFC dynamic model is interfaced to the dc-link through a boost converter as shown in Fig. 3. In this paper, operating voltage of
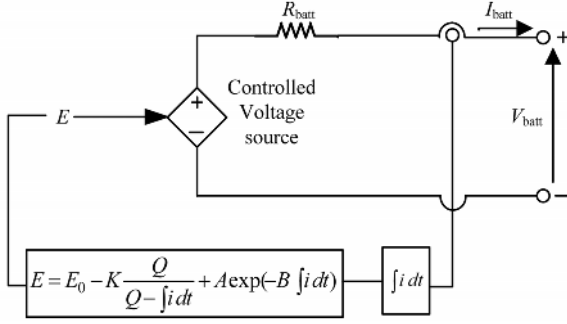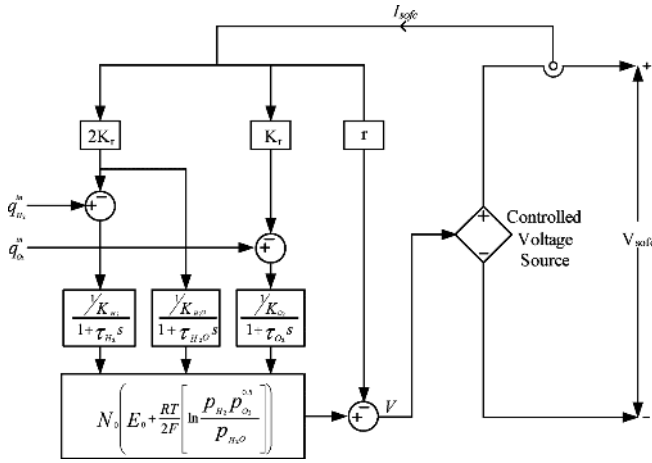
Fig. 17. Generic battery model.

Fig. 18. SOFC stack dynamic model.

SOFC is considered as 300 V and the boost converter converts it to 640 V (V_{dc}^*).

D. Electrochemical Model of Electrolyzer [24], [25]

Electrolyzer is a device to generate hydrogen from water through electrolysis. It is connected to the dc bus through a dc–dc buck converter; as a result, the input voltage and hence the current flow can be regulated. The current so drawn is used for electrolysis to produce hydrogen from water. In this paper, the buck converter switch "S_e" (Fig. 3) regulates the input voltage to the electrolyzer and switch "S_d" is regulated to feed excess power to electrolyzer so that dc link voltage is maintained.

The electrode kinetics of an electrolyzer cell can be modeled using the empirical current–voltage relationships [24]. A temperature-dependent model proposed by [24] and [25] is given as

$$V = nV_{\text{rev}} + \frac{r_1 + r_2 T}{A} I_e + (s_1 + s_2 T + s_3 T^2)$$
$$\cdot \log\left(1 + \left(t_1 + \frac{t_2}{T} + \frac{t_3}{T^2}\right) \cdot \left(\frac{I_e}{A}\right)\right) \quad (8)$$

where n is number of cells of electrolyzer, V_{rev} is the reversible cell potential (V), T is the temperature (°C), I_e/A is the current density (A/m^2), where A the cell electrode area (m^2), r_1, r_2 are the ohmic resistance parameters, $s_1, -s_3$ and $t_1 - t_3$ are overvoltage coefficients [25]. The electrochemical model of electrolyzer based on (8) is developed in MATLAB and connected
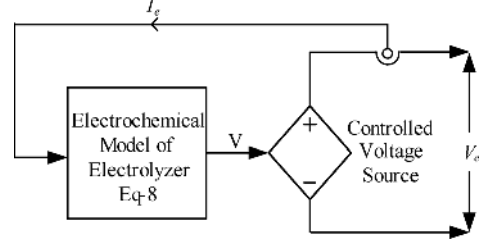

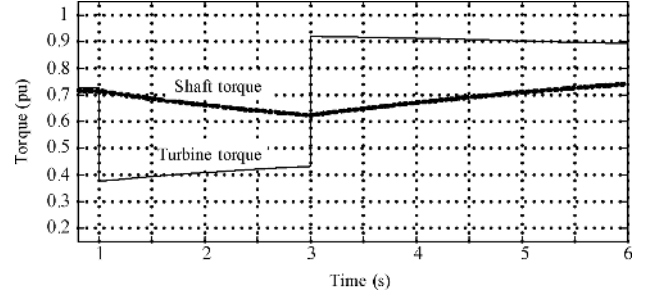Fig. 19. Electrochemical model of electrolyzer.

Fig. 20. Response of mechanical and shaft torque for change in wind velocity.

to a buck converter using controlled voltage source as shown in Fig. 19. The data of 5 kW, 120 A, 43 V electrolyzer is mentioned in [24]. In this paper, an electrolyzer of rating of about 10 kW is designed by keeping current rating at 120 A. Hence, electrolyzer voltage is considered at 86 V (by connecting 64 numbers of cells in series) and the buck converter is connected to reduce the voltage from 640 V (V_{dc}^*) to 86 V.

VI. RESULTS

The simulation model of the PMSG-based variable speed wind turbine system (shown in Fig. 3) is built using MATLAB/SIMULINK. PMSG is modeled using any arbitrary d-q reference frame [26], [27] and data is taken from [5] which are reproduced in Appendix III, where the base wind speed is considered as 12 m/s. In addition, the data of two-mass wind turbine drive train, fuel cell, and electrolyzer are also mentioned in Appendix III. The gains of all the PI controllers are tuned by the integral time square error (ITSE) method [16].

The two-mass model of drive train is incorporated in order to get a clear picture of wind turbine dynamics. The dynamics of turbine and shaft torque can be observed in Fig. 20 for the change of wind speed from 12 to 10 m/s at $t = 1$ s and from 10 to 13 m/s at $t = 3$ s. Carefully looking to Fig. 20, it can be seen that the dynamics of shaft torque is quite slow compared to that of the turbine torque. This is attributed to the two-mass model representations of the WECS. In order to observe whether WECS is following the MPPT or not, the mechanical torque is plotted in Fig. 21 for the change in wind speed from 12 to 10 m/s at $t = 1$ s. From Fig. 21, it can be found that the ratio of initial torque (at $t <= 1$ s) to that of final torque (at $t >= 15$ s) is around 1.445. The ratio so obtained is almost equal to the ratio of square of initial wind velocity (12 m/s) to that of the final wind velocity (10 m/s). Through this sample calculation it is concluded that the designed system is following the MPPT. The relation between
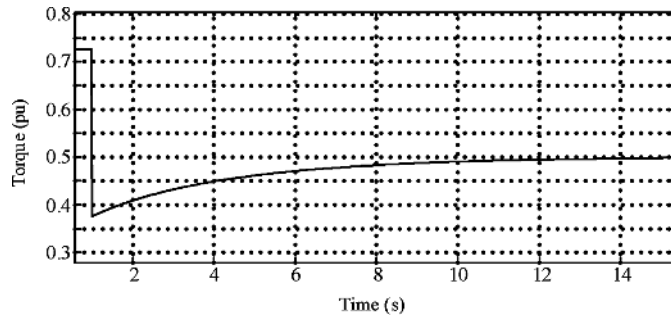
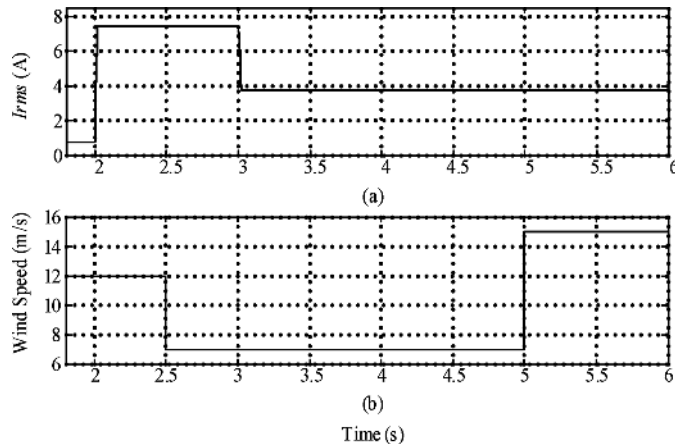Fig. 21.   Response of mechanical torque for change in wind velocity.

Fig. 23.   DC link voltage.

Fig. 22.   (a) Load current; (b) wind speed.

Fig. 24.   RMS output voltage (PCC voltage).

mechanical torque and wind velocity when MPPT is satisfied is derived in Appendix IV.

The performance of the proposed wind energy system is tested by considering the following cases:

Case-1: Considering Variations in Wind Speed and Load: In this case, the system consists of wind, battery, and dump load (i.e., electrolyzer). The instants at which the load variation is considered and its corresponding magnitude are given as follows [Fig. 22(a)]:

For 2–3 s, load current = 7.4 A.

For 3–6 s, load current = 3.7 A.

Similarly, the instant at which the wind speed is varied and its corresponding magnitude is listed as follows [Fig. 22(b)]:

For 0–2.5 s, wind speed = 12 m/s.

For 2.5–5 s, wind speed = 7 m/s.

For 5–6 s, wind speed = 15 m/s.

The dynamic response of V_{dc} for the above variations both in the load and wind speed is presented in Fig. 23. Analyzing the response of Fig. 23, it can be ascertained that the performance of the dc voltage controller both in transient as well as steady state is quite satisfactory. Further it can also be established that unlike load change when there is a variation in wind speed the dc voltage transient is almost absent. This is because of the fact that there is an appreciable delay between the PMSG output power to follow the change in wind velocity (Fig. 27). This delay is introduced into the WECS because of the more realistic two-mass model of the wind turbine. Since the delay is much higher than the response time of the dc voltage regulator, there is no change in the dc voltage following a variation in wind velocity. The output ac voltage remains constant at
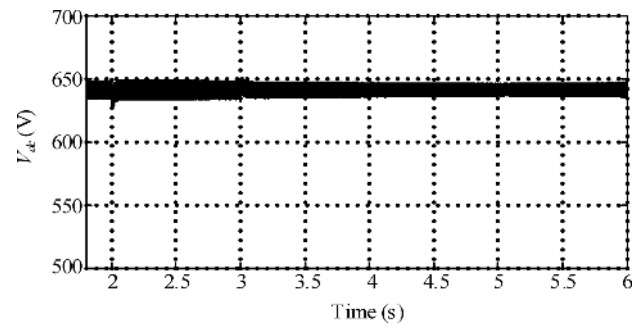

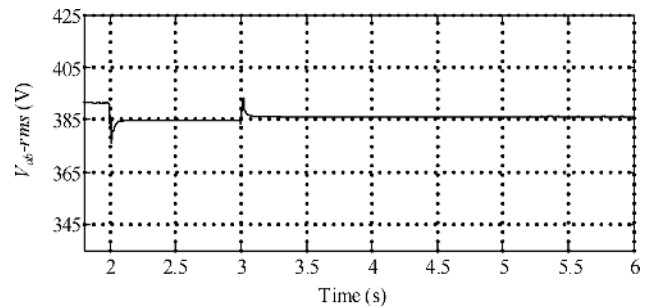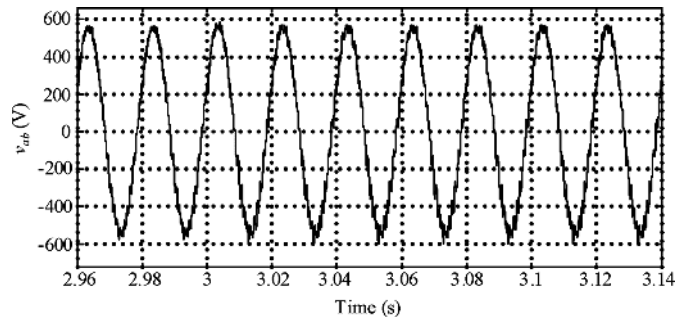Fig. 25.   Instantaneous output voltage at $t = 3$ s.

the rated value of 385 V (line-line) as shown in Fig. 24. From Fig. 24, it is observed that the output ac voltage is almost immune to fluctuations in the wind speed. However, since load is directly connected to the inverter, its variation introduces a transient in the output ac voltage. The rms value of output ac voltage may not give a clear picture of voltage waveform in the transient condition, hence instantaneous voltage is presented in Fig. 25 at $t = 3$ s. From Fig. 25, it is seen that there is no significant rise in the voltage waveform during load transient. The total harmonic distortion (THD) in the output ac voltage is about 5% in all the three phases. Similarly, it is found that the THD in line current (Fig. 26) is 5.1%. From the above simulation results, it can be established that with the help of PWM switching and a passive LC filter, a satisfactory quality of voltage as well as current can be supplied to the load.

Fig. 27 shows the power distribution between wind generator and battery for the above-mentioned load current and wind speed. From Fig. 27, it is seen that battery either delivers or absorbs the power according to the difference between the PMSG
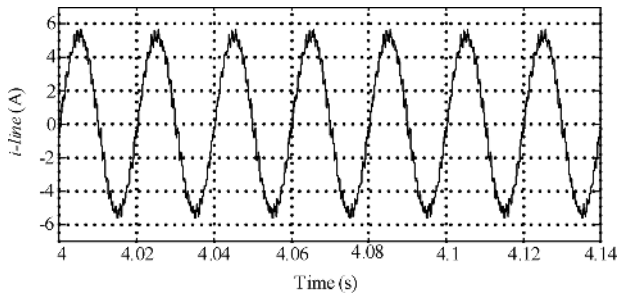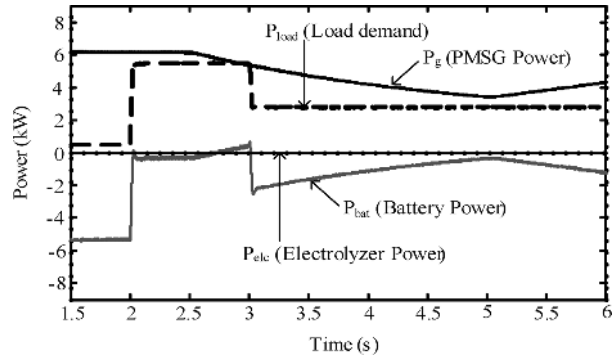
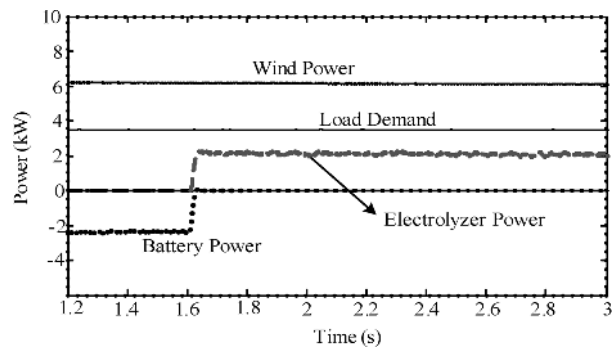Fig. 26.   Instantaneous output line current.

Fig. 27.   Powers.

Fig. 28.   Powers.

Fig. 29.   DC link voltage.

Fig. 30.   Powers.
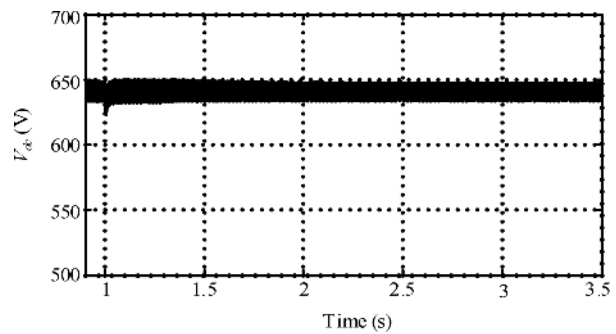
Fig. 31.   DC link voltage.
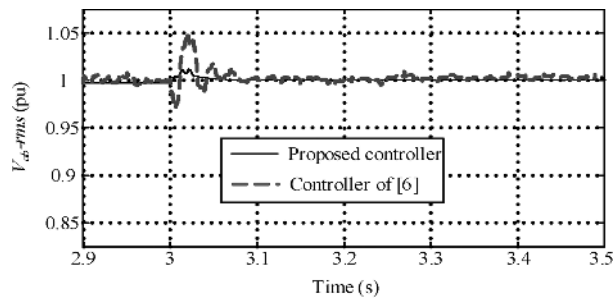
Fig. 32.   Response of controllers.

output power and load demand. In the discussed experimentation, intentionally the SOC is kept well below 0.8, so that according to Fig. 7, the aqua electrolyzer will not be switched ON.

In the second simulation, with a light load condition, the initialization of SOC of the battery is carried out near about 0.8 so that the battery will be charged due to the power mismatch and the SOC will hit the 0.8 limit. When SOC of battery becomes more than 0.8, surplus power should go to the electrolyzer which is shown in Fig. 28. From Fig. 28, it is seen that when SOC becomes more that 0.8 at $t = 1.6$ s., the electrolyzer takes over the power and battery stops charging which makes its power to zero. Fig. 29 shows the response of V_{dc} when SOC becomes more than 0.8 at $t = 1.6$ s which shows that the dc link voltage stabilizes quickly and voltage overshoot is not high and hence the safety of the dc bus is not jeopardize.

Now consider the situation when a fuel cell is connected to the dc-bus through a boost converter. For the load change from 5.5 to 9.5 kW, the response of various powers is shown in Fig. 30. From Fig. 30, it is seen that when load demand is suddenly increased at $t = 1$ s, battery responses instantaneously to meet the load demand. Since fuel cell dynamics is slow, it feeds the

power slowly. Through the control scheme proposed in Figs. 4 and 6, it is achieved that as fuel cell power increases to meet the load demand, battery power decreases (Fig. 30). Hence, through this, the control battery is used to meet the load demand only in the transient condition. Fig. 31 shows the response of V_{dc} which depicts a stable dc link voltage.

Fig. 32 compares the dynamic response of the proposed controller and the one mentioned in [5] and [6], for a change in load.
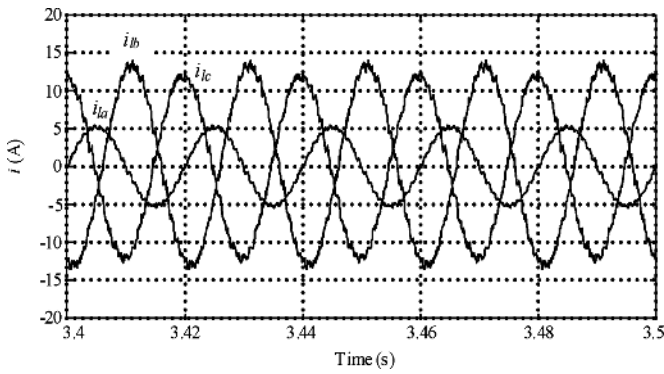
Fig. 33.   Three phase currents for unbalanced load.

Fig. 34.   Electrical torque of PMSG with and without dc–dc converter controller.

Fig. 35.   Instantaneous line voltages at PCC for unbalanced load.

Fig. 36.   (a) RMS value of line voltages at PCC after compensation; (b) modulation indexes.

Fig. 37.   Instantaneous line voltages at PCC after compensation.

The response of the proposed controller is approximately similar to that discussed in [5] and [6]. However, as they have used five PI controllers instead of a single one as proposed (battery controller, Fig. 4), the tuning of the controller parameters will be a tedious task.

Case-2: Considering Unbalanced Load: Consider the unbalanced load currents for three phases (Fig. 33) as mentioned as follows:

$$i_{la} = 3.53 \text{ A}; \quad i_{lb} = 9.55 \text{ A}; \quad i_{lc} = 8.45 \text{ A}.$$
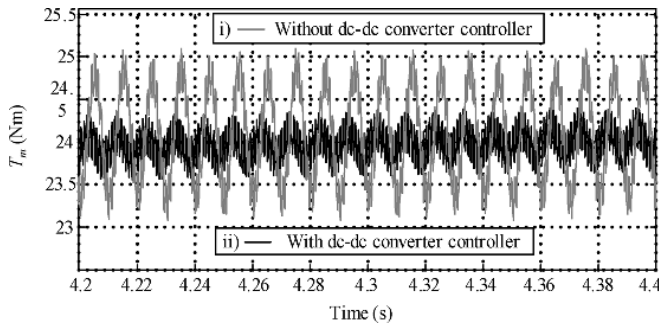
Fig. 34 compares the variation of electrical torque of the PMSG with and without the dc–dc converter associated with the battery. It can be found from Fig. 34 that by proper control of the dc–dc converter (Fig. 8), it is possible to reduce the torque pulsation drastically. Hence, proposed dc–dc converter controller is not only maintaining V_{dc} constant but also acts as a dc-side active filter and reduces the oscillations in the electrical torque of the generator.

Further, due to the above-mentioned unbalanced load (Fig. 33), the line voltages at PCC (Fig. 35) also exhibits some unbalance behavior. The voltage unbalance factor (VUF), i.e., ratio of negative to positive sequence of the fundamental component is found to be 2.6% which is greater than the permissible limit (i.e., 1%). To reduce VUF to an acceptable limit, the proposed PWM inverter control is applied and the VUF is brought down to 0.4%. The rms values of line voltages and modulation indices for all three phases are depicted in Fig. 36. The instantaneous line voltages are shown in Fig. 37. The THD in v_{ab}, v_{bc}, and v_{ca} are 5%, 3.9%, and 5.3%, respectively, which are well below the acceptable limit.
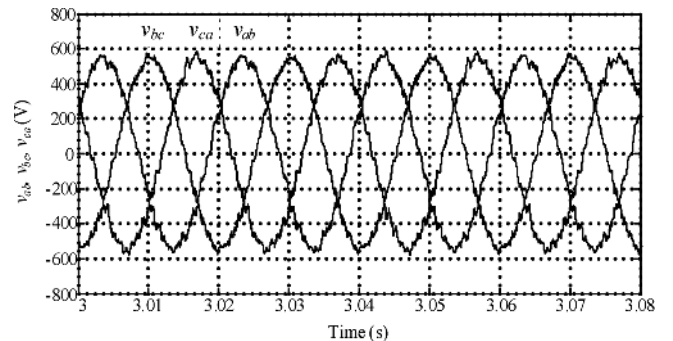
VII. DISCUSSION

When the proposed system will be considered for grid connection, we foresee the following.

  i) The PMSG will be always under MPPT like the present scenario.

 ii) The battery, fuel cell and aqua electrolyzer will be required only if we need to feed a scheduled power to the grid which is not the same as the maximum power available from the wind.

iii) Since grid frequency can be a variable one we have to synchronize the inverter output frequency with the grid. This can be achieved by measuring the frequency of the grid using PLL and accordingly deciding the frequency of reference signal given to the grid-side PWM inverter.

iv) As there is a grid side inverter, it can supply reactive power to the grid whenever required for voltage support. However, this benefit will be limited based on the capacity margin available with inverter at that instant.

VIII. Conclusion

Control strategies to regulate voltage of a standalone variable speed wind turbine with a PMSG, battery, fuel cell, and electrolyzer (acts as dump load) are presented in this paper. By maintaining dc link voltage (V_{dc}) at its reference value and controlling modulation indices of the PWM inverter, the voltage of inverter output is maintained constant at their rated values. From the simulation results, it is seen that the controller can maintain the load voltage quite well in spite of variations in wind speed and load. An algorithm is developed to achieve intelligent energy management among the wind generator, battery, fuel cell, and electrolyzer.

The effect of unbalanced load on the generator is analyzed and the dc–dc converter control scheme is proposed to reduce its effect on the electrical torque of the generator. The dc–dc converter controller not only helps in maintaining the dc voltage constant but also acts as a dc-side active filter and reduces the oscillations in the generator torque which occur due to unbalanced load. PWM inverter control is incorporated to make the line voltage at PCC balanced under an unbalanced load scenario. Inverter control also helps in reducing PCC voltage excursion arising due to slow dynamics of aqua elctrolyzer when power goes to it. The total harmonic distortion (THD) in voltages at PCC is about 5% which depicts the good quality of voltage generated at the customer end. The simulation results demonstrate that the performance of the controllers is satisfactory under steady state as well as dynamic conditions and under balanced as well as unbalanced load conditions.

Appendix I

Calculation for battery rating $=$ (6 kW × 1 hr/300 V × 0.6) = 33.33 Ahr.

Hence, 35-Ahr 12-V battery rating is considered and, therefore, 25 numbers of batteries are required to connect in series.

Appendix II

The $L - C$ filter design is based on following equations [11]:

$$K = \left[\left(k^2 - \frac{15}{4}k^4 + \frac{64}{5\pi}k^5 - \frac{5}{4}k^6 \right) \Big/ 1440 \right]^{1/2} \quad (9)$$

$$L_f = \frac{V_o}{I_o f_s} \left\{ K \frac{V_{dc}}{V_{o,av}} \left[1 + 4\pi^2 \left(\frac{f_r}{f_s} \right)^2 K \frac{V_{dc}}{V_{o,av}} \right] \right\}^{1/2} \quad (10)$$

$$C_f = K \frac{V_{dc}}{L_f f_s^2 V_{o,av}} \quad (11)$$

where
k	(modulation index) = 1;
V_o	(Load voltage) = $385/\sqrt{3}$ V;
I_o	(Nominal current) = 10 A;
f_r	(Fundamental frequency) = 50 Hz;
f_s	(Switching frequency) = 3 kHz;

$V_{o,av}$	(Total harmonic load voltage) = 5% of V_o;
L_f	= Inductance of filter;
C_f	= Capacitance of filter.

Appendix III
Parameters of PMSG

Number of poles	10
Rated speed	153 rad/s
Armature resistance (R_s)	0.425 Ω
Magnetic flux linkage	0.433 Wb
Stator inductance (L_s)	8.4 mH
Rated torque	40 Nm
Rated power	6 kW

Parameters of Two Mass Drive Train

H_t ; H_g	4s ; 0.1H_t
K_{sh}	0.3 p.u./el.rad
D_t	0.7 p.u.s/el.rad

Parameters of Fuel Cell

Absolute temperature (T)	1273K
Faraday's constant (F)	96487C/kmol
Universal gas constant (R)	8314J/(kmol K)
Ideal standard potential (E_0)	1.18V
Number of cells in series in stack (N_0)	325
Constant, $K_r=N_0/4F$	$0.842*10^{-6}$ kmol/(s A)
Valve molar constant for hydrogen (K_{H_2})	$8.43*10^{-4}$ (kmol/(s atm))
Valve molar constant for water (K_{H_2O})	$2.81*10^{-4}$ (kmol/(s atm))
Valve molar constant for oxygen (K_{O_2})	$2.52*10^{-3}$ (kmol/(s atm))
Response time for hydrogen flow (τ_{H_2})	26.1 s
Response time for water flow (τ_{H_2O})	78.3 s
Response time for oxygen flow (τ_{O_2})	2.91 s
Ohmic loss/cell (r)	$32813*10^{-8}$ Ω

Parameters of Electrolyzer

r_1	0.0015 Ω m^2
r_2	$-6.019*10^{-6}$ m^2 ^{0}C^{-1}
s_1	2.427 V
s_2	-0.0307 V ^{0}C^{-1}
s_3	$3.90*10^{-4}$ V ^{0}C^{-2}
t_1	0.214 A^{-1} m^2
t_2	-9.870 A^{-1} m^2 ^{0}C
t_3	119.1 A^{-1} m^2 ^{0}C^2
N	64
V_{rev}	1.1647 V
T	70 ^{0}C
A	873 cm^2

Appendix IV

The amount of power captured by wind turbine is given by

$$P_t = 0.5\rho A C_p(\lambda, \beta)v^3 \quad (12)$$

where ρ is air density, v is wind speed, A is blade's swept area, and C_p is turbine-rotor power coefficient

$$T_m = \frac{P_t}{\omega_t} \quad (13)$$

and

$$\lambda = \frac{\omega_t}{v}.$$

For maximum power tracking, $\lambda = \lambda_{\mathrm{opt}} = \text{constant}$

$$\therefore \frac{\omega_{t_1}}{v_1} = \frac{\omega_{t_2}}{v_2}. \quad (14)$$

Moreover, if WECS is under MPPT in steady state, $C_p = \text{constant} = 1$ p.u., and ρ, A are constant

$$\therefore T_m \propto \frac{v^3}{\omega_t}. \quad (15)$$

Putting (14) in (15) and taking ratio of torque at two wind velocities, we get

$$\frac{T_{m1}}{T_{m2}} = \frac{v_1^3}{v_2^3} \times \frac{v_2}{v_1} = \frac{v_1^2}{v_2^2}. \quad (16)$$

Hence, (16) denotes relation between torque and wind velocity when WECS is under MPPT.

References

[1] S. Müller, M. Deicke, and W. De DonckerRik, "Doubly fed induction generator system for wind turbines," *IEEE Ind. Appl. Mag.*, vol. 8, no. 3, pp. 26–33, May/Jun. 2002.
[2] H. Polinder, F. F. A. van der Pijl, G. J. de Vilder, and P. J. Tavner, "Comparison of direct-drive and geared generator concepts for wind turbines," *IEEE Trans. Energy Convers.*, vol. 21, no. 3, pp. 725–733, Sep. 2006.
[3] T. F. Chan and L. L. Lai, "Permanent-magnet machines for distributed generation: A review," in *Proc. 2007 IEEE Power Engineering Annual Meeting*, pp. 1–6.
[4] M. Fatu, L. Tutelea, I. Boldea, and R. Teodorescu, "Novel motion sensorless control of stand alone permanent magnet synchronous generator (PMSG): Harmonics and negative sequence voltage compensation under nonlinear load," in *Proc. 2007 Eur. Conf. Power Electronics and Applications*, Aalborg, Denmark, Sep. 2–5, 2007.
[5] M. E. Haque, K. M. Muttaqi, and M. Negnevitsky, "Control of a stand alone variable speed wind turbine with a permanent magnet synchronous generator," in *Proc. IEEE Power and Energy Society General Meeting*, Jul. 2008, pp. 20–24.
[6] M. E. Haque, M. Negnevitsky, and K. M. Muttaqi, "A novel control strategy for a variable-speed wind turbine with a permanent-magnet synchronous generator," *IEEE Trans. Ind. Appl.*, vol. 46, no. 1, pp. 331–339, Jan./Feb. 2010.
[7] N. Mohan, T. M. Undeland, and W. P. Robbins, *Power Electronics: Converters, Applications, and Design*. Hoboken, NJ: Wiley, 2002.
[8] *IEEE Guide for Optimizing the Performance and Life of Lead-Acid Batteries in Remote Hybrid Power Systems*, IEEE Std. 1561-2007.
[9] D. M. Whaley, W. L. Soong, and N. Ertugrul, "Investigation of switched-mode rectifier for control of small-scale wind turbines," in *Proc. IEEE Industry Applications Society Annual Meeting*, 2005, pp. 2849–2856.
[10] E. Muljadi, S. Drouilhet, R. Holz, and V. Gevorgian, "Analysis of permanent magnet generator for wind power battery charging," in *Proc. IEEE Industry Applications Society Annual Meeting*, 1996, pp. 541–548.
[11] P. A. Dahono and A. Purwadi, Qamaruzzaman, "An LC filter design method for single-phase PWM inverters," in *Proc. Int. Conf. Power Electronics and Drive Systems*, 1995, vol. 2, pp. 571–576.
[12] A. M. Cross, P. D. Evans, and A. J. Forsyth, "DC link current in PWM inverters with unbalanced and non-linear loads," in *Proc. Inst. Elect. Eng. Electrical Power Applications*, Nov. 1999, vol. 146, no. 6, pp. 620–626.
[13] P. Enjeti and S. Kim, "A new DC-side active filter for inverter power supplies compensates for unbalanced and nonlinear loads," in *Proc. IEEE Industry Applications Society Annual Meeting*, 1991, vol. 1, pp. 1023–1031.
[14] D.-M. Lee, T. G. Habetler, R. G. Harley, T. L. Keister, and J. R. Rostron, "A voltage sag supporter utilizing a PWM-switched autotransformer," *IEEE Trans. Power Electron.*, vol. 22, no. 2, pp. 626–635, Mar. 2007.
[15] H.-Y. Chu, H.-L. Jou, and C.-L. Huang, "Transient response of a peak voltage detector for sinusoidal signals," *IEEE Trans. Ind. Electron.*, vol. 39, no. 1, pp. 74–79, Oct. 1992.
[16] C. N. Bhende, S. Mishra, and S. K. Jain, "TS-fuzzy-controlled active power filter for load compensation," *IEEE Trans. Power Del.*, vol. 21, no. 3, pp. 1459–1465, Jul. 2006.
[17] I. Vechiu, O. Curea, and H. Camblong, "Transient operation of a four-leg inverter for autonomous applications with unbalanced load," *IEEE Trans. Power Electron.*, vol. 25, no. 2, pp. 399–407, Feb. 2010.
[18] A. Mohd, E. Ortjohann, N. Hamsic, W. Sinsukthavorn, M. Lingemann, A. Schmelter, and D. Morton, "Control strategy and space vector modulation for three-leg four-wire voltage source inverters under unbalanced load conditions," *IET Power Electron.*, vol. 3, pp. 323–333, 2010.
[19] I. Vechiu, H. Camblong, G. Tapia, B. Dakyo, and O. Curea, "Control of four leg inverter for hybrid power system applications with unbalanced load," *Energy Convers. Manage.*, vol. 48, pp. 2119–2128, 2007.
[20] F. Mei and B. Pal, "Modal analysis of grid-connected doubly fed induction generators," *IEEE Trans. Energy Convers.*, vol. 22, no. 3, pp. 728–736, Sep. 2007.
[21] O. Tremblay, L.-A. Dessaint, and A.-I. Dekkiche, "A generic battery model for the dynamic simulation of hybrid electric vehicles," in *Proc. 2007 IEEE-Vehicle Power and Propulsion Conf.*, Arlington, TX, Sep. 9–13, 2007.
[22] J. Padulles, G. W. Ault, and J. R. McDonald, "An integrated SOFC plant dynamic model for power systems simulation," *J. Power Sources*, vol. 86, pp. 495–500, 2000.
[23] Y. Zhu and K. Tomsovic, "Development of models for analyzing the load-following performance of microturbines and fuel cells," *Elect. Power Syst. Res.*, vol. 62, pp. 1–11, 2002.
[24] P. M. Dieguez, A. Ursua, P. Sanchis, C. Sopena, E. Guelbenzu, and L. M. Gandia, "Thermal performance of commercial alkaline water electrolyzer: Experimental study and mathematical modeling," *Int. J. Hydrogen Energy*, vol. 33, pp. 7338–7354, 2008.
[25] O. Ulleberg, "Modeling of advanced alkaline electrolyzers: A system simulation approach," *Int. J. Hydrogen Energy*, vol. 28, pp. 21–33, 2003.
[26] D. Grenier, L.-A. Dessaint, O. Akhrif, Y. Bonnassieux, and B. LePioufle, "Experimental nonlinear torque control of a permanent magnet synchronous motor using saliency," *IEEE Trans. Ind. Electron.*, vol. 44, no. 5, pp. 680–687, Oct. 1997.
[27] P. C. Krause, O. Wasynczuk, and S. D. Sudhoff, *Analysis of Electrical Machinery and Drive System*. Piscataway, NJ: IEEE Press, 2002.

C. N. Bhende received the Ph.D. degree from Indian Institute of Technology Delhi, India, in 2008.

In June 2008, he went to the University of Wollongong, Australia, for Postdoctoral Research and in December 2008, he became an Assistant Professor at the Indian Institute of Technology Guwahati, India. Presently, he is a faculty member at the School of Electrical Sciences, Indian Institute of Technology Bhubaneswar, India. His field of interest includes power quality, custom power devices, and renewable energy sources.

Dr. Bhende has been honored with the prestigious Innovative Ph.D. Thesis Award in 2009 by INAE.

S. Mishra (M'97–SM'04) received the B.E. degree from University College of Engineering, Burla, Orissa, India, in 1990, and the M.E. and Ph.D. degrees from Regional Engineering College, Rourkela, Orissa, India, in 1992 and 2000, respectively.

In 1992, he joined the Department of Electrical Engineering, University College of Engineering Burla as a Lecturer, and subsequently became a Reader in 2001. Presently, he is an Associate Professor with the Department of Electrical Engineering, Indian Institute of Technology Delhi, India. His interests are in soft computing applications to power system control, power quality, and renewable energy.

Dr. Mishra has been honored with many prestigious awards such as the INSA Young Scientist Medal in 2002, INAE Young Engineer's Award in 2002, and recognition as the DST Young Scientist in 2001 to 2002, etc. He is a Fellow of Indian National Academy of Engineering and Institute of Electronics and Telecommunication Engineering.

Siva Ganesh Malla received the B.Tech. and M.Tech. degrees from Jawaharlal Nehru Technological University, in 2007 and 2010, respectively. He is currently working toward the Ph.D. degree in the School of Electrical Sciences, Indian Institute of Technology Bhubaneswar, India.